Zonal Circulations over the Equatorial Indian Ocean

STEFAN HASTENRATH

Department of Atmospheric and Oceanic Sciences, University of Wisconsin—Madison, Madison, Wisconsin

(Manuscript received 29 July 1999, in final form 5 November 1999)

ABSTRACT

The NCEP–NCAR 1958–97 upper-air dataset and surface observations have been analyzed for evidence of zonal–vertical circulations along the Indian Ocean equator and their role in climatic variability. The long-term mean upper-tropospheric circulation is dominated in boreal winter by divergent outflow from the southern Indian Ocean northwestward into southern Asia, and in summer from southern Asia southwestward into the Southern Hemisphere. In boreal autumn only, divergent easterlies blow from Indonesia along the equator into an upper-tropospheric convergence band over East Africa, and only then a closed zonal–vertical circulation cell materializes along the Indian Ocean equator, between the centers of ascending motion over Indonesia and of subsidence over equatorial East Africa, and featuring westerlies in the lower layers. The boreal autumn zonal–vertical circulation varies interannually. A regime of intense circulation features accelerated equatorial surface westerlies, enhanced subsidence, and deficient rainfall at the coast of East Africa. In the high phase of the Southern Oscillation [anomalously high (low) pressure at Tahiti (Darwin)] this regime is preferred. The regime of weak zonal circulation has the opposite departure characteristics.

1. Introduction

In a seminal paper Bjerknes (1969) postulated a circulation cell in the vertical-equatorial plane over the Pacific, which he named ''Walker Circulation.'' The dynamics of this cell pertain to the near vicinity of the equator, where the Coriolis acceleration vanishes and the balance is between the pressure gradient and frictional accelerations. A series of subsequent publications hypothesized corollaries for other longitudes around the globe (review in Hastenrath 1995, pp. 198–201). Thus Flohn (1971) inferred four zonal circulation cells along the equator from the zonal profiles of sea surface temperature (SST) and satellite-inferred convection. Newell (1979) deduced five equatorial circulation cells from wind observations (Newell et al. 1972, 1974, p. 151), and Chervin and Druyan (1984) simulated these in numerical modeling experiments. Krishnamurti (1971) and Krishnamurti et al. (1973) analyzed the circumglobal 200-mb wind field for one winter and one summer season to infer zonal circulation cells in broad bands away from the equator. In the process Krishnamurti (1971) pioneered the analysis method appropriate for the study of divergent flow.

With this backgroud it appears tempting to surmise that zonal equatorial circulations play a major role for the climatic variability at the western and eastern extremities of the Indian Ocean basin. Reverdin et al. (1986) called attention to the interannual variability of surface winds over the equatorial Indian Ocean. For the coast of eastern Africa, Ogallo (1988), Ogallo et al. (1988), Farmer (1988), Hutchinson (1992), and Beltrando and Camberlin (1993) pointed out an association of the boreal autumn rains with the Southern Oscillation (SO), with the precipitation deficient during the high SO phase [defined by anomalously high (low) pressure at Tahiti (Darwin)]. Also pertaining to the rainfall variability of the region are the studies by Ropelewski and Halpert (1987, 1989) and Janowiak (1988). Farmer (1988) and Hutchinson (1992) further demonstrated that a modest portion of the rainfall variability in boreal autumn can be predicted from the Tahiti minus Darwin presssure index alone. For the boreal spring rainy season associations are weak. Hastenrath et al. (1993) found a concurrent correlation between the boreal autumn rains at the coast of equatorial East Africa and the October/November surface westerlies over the equatorial Indian Ocean of -0.85, significant at the 1% level. This unusually strong and, over decades, robust correlation is, however, not helpful in climate prediction, for lack of precursors in the seasonal evolution. The equatorial westerlies tend to be faster during the high SO phase. In the boreal spring rainy season of equatorial East Africa, the associations of the equatorial surface westerlies with regional rainfall and SO are weak. The westerly

Corresponding author address: Dr. Stefan Hastenrath, Dept. of Atmospheric and Oceanic Sciences, University of Wisconsin—Madison, 1225 West Dayton St., Madison, WI 53706.
E-mail: barafu@macc.wisc.edu

surface winds along the Indian Ocean equator are limited to April–May and October–November (Hastenrath and Lamb 1979b, charts 14–25), and they may be perceived as lower-tropospheric manifestations of a zonal circulation cell. Such perceptions shall be explored from upper-air analyses along with surface observations. It is recognized that the National Centers for Environmental Prediction–National Center for Atmospheric Research (NCEP–NCAR) dataset (Kalnay et al. 1996) used here is based on the model assimilation of diverse observations; application to an important circulation problem provides insight into the potential and limitations of this product. Section 2 summarizes the data sources and the analysis procedures, section 3 discusses the long-term mean circulation, section 4 the interannual variability, and a synopsis is presented in the closing section 5.

2. Data and analysis

Global upper-air analyses and surface ship observations are the main data sources for this study.

The NCEP–NCAR reanalysis (Kalnay et al. 1996; Kousky and Ropelewski 1997) at a 2.5° lat × 2.5° long resolution was acquired for the years 1958–97. Data were processed into individual monthly mean fields. Elements of interest here are the fields of wind and vertical velocity for the levels surface (10 m), 1000, 925, 850, 700, 600, 500, 400, 300, 200, and 100 mb.

Surface ship observations stemming from the same TDF-11 dataset as used in our atlases (Hastenrath and Lamb 1979a,b) are available in the Comprehensive Ocean–Atmosphere Dataset (COADS) collection, with spatial resolutions of 2° and 1° latitude–longitude squares (Woodruff et al. 1987, 1993).

From the total wind field at selected levels, velocity potential and streamfunction were computed as described in Mancuso (1967), Krishnamurti (1971), and Krishnamurti et al. (1973), with full coverage from 75°N to 75°S and a grid spacing of 2.5°. An inner subdomain from these near-global fields is used here (Fig. 1a). Maps of divergent wind component and divergence were then constructed from the fields of velocity potential.

The data sources described above were evaluated in a variety of ways. A selection of these analyses is reproduced here. Essential for the study of circulation cells in the Tropics is the analysis of the divergent part of the wind field and of divergence at various levels and especially in the upper troposphere. From this, one obtains the fields of vertical motion, especially in the mid-troposphere. In light of the implied dynamics of the Walker circulation (Bjerknes 1969), zonal-vertical transects are appropriate for a narrow latitude strip in the near vicinity of the equator. These may combine the distributions of vertical motion and of the zonal component of the divergent part of the wind field. However, this is not sufficient to discern closed circulation cells: while having a zonal component, the divergent flow may not be directed along the equator but substantially across

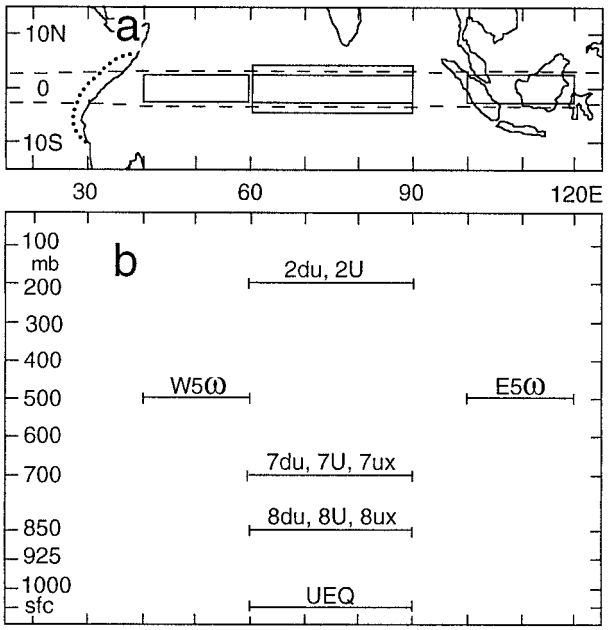

FIG. 1. Orientation map and cross section. (a) In the map, dashed lines enclose the latitude strip 2.5°N–2.5°S of the zonal–vertical cross sections in Figs. 1b, 3, and 6. The area pertaining to the rainfall indices RAM and RON is bounded by a dotted line. Solid-line rectangles indicate the domains detailed in the transect b. (b) The cross section shows the levels and longitude domains within the latitude strip 2.5°N–2.5°S for which circulation indices were compiled: W5ω and E5ω are omega vertical velocity at 500 mb at 40°–60°E and 100°–120°E, respectively, and are representative of the vertical motion at the western and eastern extremities of the Indian Ocean basin. Here 2*du* and 2*U* are the divergent part of the zonal wind and total zonal wind, respectively, at 200 mb and 60°–90°E; they represent the upper-tropospheric flow between the centers of strongest vertical motion. Here 7*du* and 7*U* are the same as 2*du* and 2*U* for 700 mb, and 8*du* and 8*U* the same for 850 mb; they describe the corresponding opposite-directed flow in the mid- to lower troposphere. UEQ is the surface zonal wind at 4°N–4°S and 60°–90°E.

it. This may be appreciated from maps of the divergent flow at indicative levels. Accordingly, maps are presented here for a limited equatorial domain (15°N–15°S and 15°–125°E) along with zonal-vertical transects for the narrow zonal strip 2.5°N–2.5°S.

Several indices were used to mark conditions of circulation and climate. Ten upper-air circulation indices were compiled from the NCEP–NCAR dataset, as detailed in the caption to Fig. 1b. SOI is the pressure difference at Tahiti minus Darwin and represents an index of the SO. Precipitation at the coast of East Africa at the April–May and October–November rainy season peaks is described by the indices RAM and RON, respectively. They are the all-station average normalized departures at a network of seven coastal stations (Fig. 1a). UEQ is the surface westerly wind component in the domain 4°N–4°S and 60°–90°E, obtained from ship observations. For October, ensembles of 10 extreme years each were identified from the indices SOI, RON, and UEQ. The years of the high SO phase are 1962,

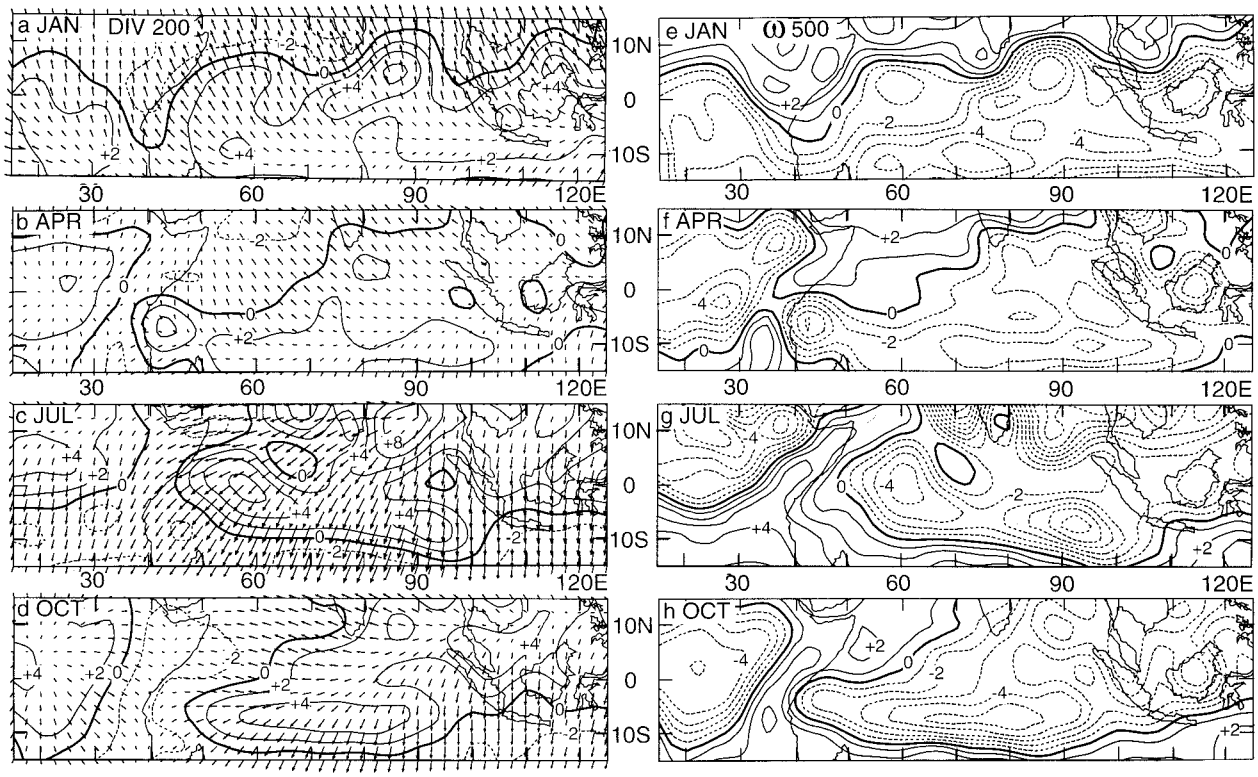

FIG. 2. Maps of 1958–97 mean upper-air circulation in (a) and (e) Jan, (b) and (f) Apr, (c) and (g) Jul, and (d) and (h) Oct. Maps (a)–(d) present the 200-mb field of divergent wind with arrows scaled at 1° lat for 2 m s^{-1}. Divergence is shown with isoline spacing of 2×10^{-6} s^{-1} and dashed lines indicating negative values. Maps (e) and (f) depict vertical motion at 500 mb, with isoline spacing of 10^{-4} mb s^{-1} and dashed lines indicating negative values or upward motion.

1964, 1970, 1971, 1973, 1974, 1975, 1986, 1988, 1989; and those of the low SO phase 1963, 1969, 1977, 1982, 1987, 1991, 1992, 1993, 1994, 1997 (index SOI). The years of dry conditions at the coast of East Africa are 1958, 1959, 1962, 1964, 1970, 1971, 1975, 1979, 1983, 1987; and those of wet conditions 1961, 1963, 1965, 1967, 1968, 1972, 1977, 1978, 1982, 1994 (index RON). The years with fast surface westerlies over the equatorial Indian Ocean are 1958, 1964, 1970, 1974, 1975, 1983, 1988, 1993, 1995, 1996; and those with slow westerlies 1961, 1963, 1965, 1967, 1972, 1977, 1983, 1988, 1993, 1995, 1996 (index UEQ).

In the significance testing of correlation coefficients, Quenouille's (1952, p. 182) method was used to account for the reduction of the effective number of degrees of freedom due to persistence. The significance of differences between ensembles was ascertained using Student's *t* test.

3. Long-term mean conditions

The 1958–97 mean upper-air circulation as captured by the NCEP–NCAR dataset is presented here by maps of indicative fields (Fig. 2) and zonal–vertical cross sections (Fig. 3) for the months January, April, July, and October, and by diagrams of the complete annual cycle of representative indices (Fig. 4).

The maps in Fig. 2 show the fields of upper-tropospheric divergence and divergent wind component (200 mb, Figs. 2a–d) and of midtropospheric vertical motion (500 mb, Figs. 2e–h). In January (Figs. 2a and 2e), divergent outflow in the upper troposphere is directed from the Southern Hemisphere and the equatorial zone broadly northwestward into a domain of convergence extending from equatorial East Africa to the northern edge of the map area. Concordant with the upper-tropospheric divergence and divergent flow pattern (Fig.

→

FIG. 3. Zonal–vertical cross sections at 2.5°N–2.5°S along the equator for the 1958–97 mean in (a) and (e) Jan, (b) and (f) Apr, (c) and (g) Jul, and (d) and (h) Oct. Cross sections (a)–(d) present the zonal circulation, with inset in (a) indicating the scaling of arrows (m s^{-1}) for the divergent zonal wind component and (10^{-4} mb s^{-1}) for the omega vertical velocity. Stippling distinguishes domains of convergence from those of divergence, with thin solid lines enclosing values beyond 1×10^{-6} s^{-1} in absolute amount (+ or −). Cross sections (e)–(h) depict total zonal wind component with isotach spacing of 2 m s^{-1} and dashed lines indicating flow from the east.

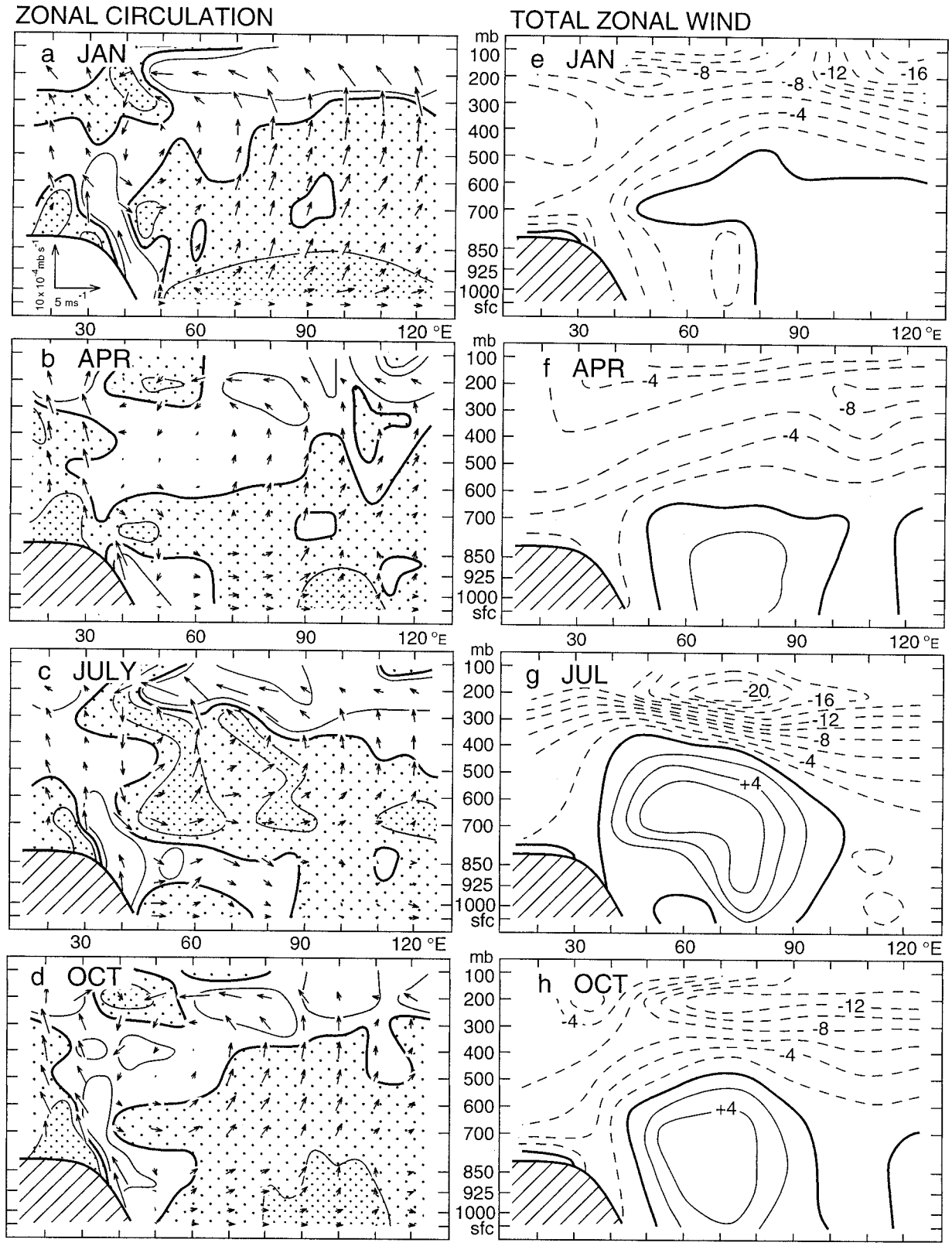

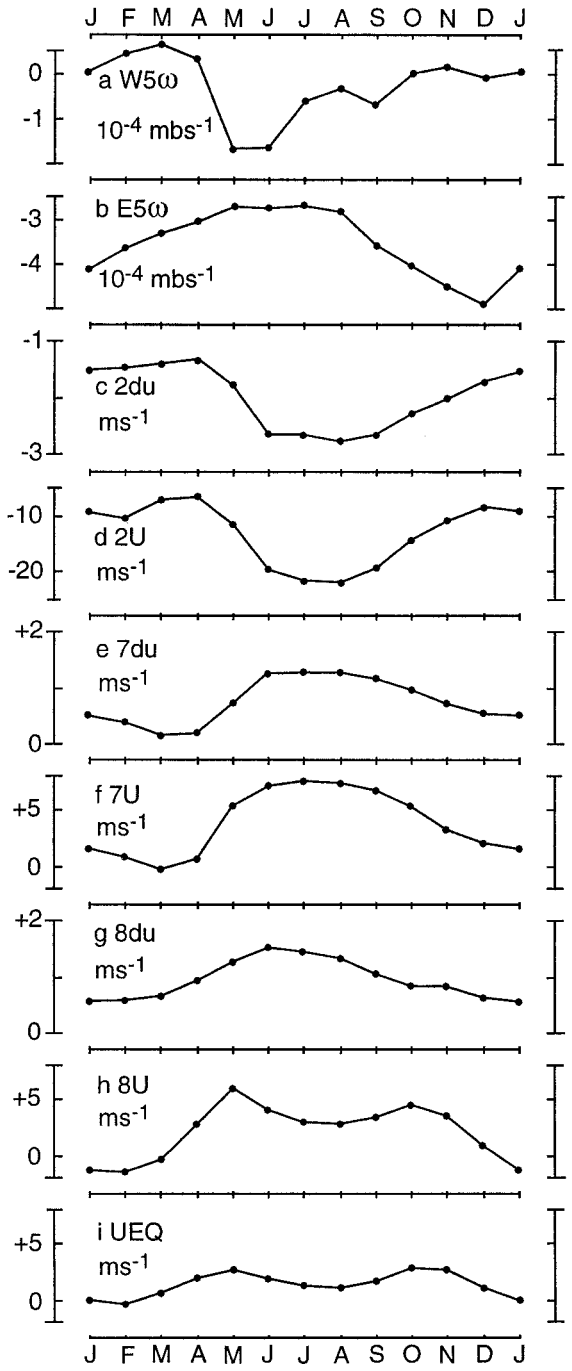

FIG. 4. Annual cycle of zonal circulation, 1958–97 mean with indices defined in caption to Fig. 1. Note that (a) and (b) for vertical motion have the same vertical scale; (c), (e), and (g) for divergent part of zonal flow have vertical scale 10 times that for total zonal flow in (d), and 5 times that for total zonal flow in (f), (h), and (i). (a) W5ω (10^{-4} mb s^{-1}). (b) E5ω (10^{-4} mb s^{-1}). (c) 2*du* (m s^{-1}). (d) 2*U* (m s^{-1}). (e) 7*du* (m s^{-1}). (f) 7*U* (m s^{-1}). (g) 8*du* (m s^{-1}). (h) 8*U* (m s^{-1}). (i) UEQ (m s^{-1}).

2a), midtropospheric upward motion is strongest in a zone around 10°S and subsidence is confined to the northern part of the map area and East Africa (Fig. 2e). In April (Figs. 2b and 2f), upper-tropospheric divergence prevails in the eastern to central part of the map area with largest values over Indonesia and the southern Indian Ocean, while convergence is found over East Africa and the Arabian Sea. The divergent flow has a substantial easterly component in the equatorial zone, except to the west of about 60°E. Concordant with the upper-tropospheric divergence pattern, ascending motion prevails in most of the map area with largest values over Indonesia, the southern Indian Ocean, and Central Africa, while subsidence is found over East Africa and the Arabian Sea. In July (Figs. 2c and 2g), the upper troposphere is dominated by the broadly southwestward-directed divergent outflow from the South Asian monsoon region, with convergent inflow taking place into eastern Africa and the southern Indian Ocean. Subsidence is found in a distinct southwest–northeast-oriented band extending from eastern Africa to the Arabian Sea, while ascending motion prevails in most of the map area. October (Figs. 2d and 2h) features the transition from the boreal summer to the winter monsoon. Particularly prominent is a broad band over eastern Africa and the Arabian Sea into which upper-tropospheric convergent inflow takes place from the central Indian Ocean and from central Africa. Divergence is largest over Indonesia and the southern Indian Ocean. The divergent easterly flow along the equator over the central Indian Ocean is best developed in this season, and much stronger than in April (Figs. 2g and 2f), while in boreal winter and summer (Figs. 2e and 2g) the divergent part of the wind field has a strong meridional component. Concordant with the map of upper-tropospheric divergence and divergent wind component (Fig. 2d), a southwest–northeast-oriented band of subsidence extends from eastern Africa to the Arabian Sea, while centers of strongest upward motion are found over Central Africa, the southern Indian Ocean and Indonesia.

The cross sections (Fig. 3) documenting the circulation in the zonal-vertical plane along the Indian ocean equator should be viewed in the context of the maps (Fig. 2). In particular, Figs. 3a–d synthesize the evidence on vertical motion, divergence, and zonal component of the divergent part of the wind field, while Figs. 3e–h depict the total zonal wind component. In January (Figs. 3a and 3e), the eastern extremity of the transect, or Indonesia, demonstrates the greatest lower-tropospheric convergence, strong ascending motion and upper-tropospheric divergence, and divergent outflow (Fig. 2a), directed in part westward (although more prominently northward). At the western extremity of the Indian Ocean basin, there is upper-tropospheric convergent inflow with a westward component (Fig. 3a), subsidence, divergence in the mid- to lower troposphere, and divergent outflow eastward concentrated around 700 mb. The cross section of total zonal flow (Fig. 3e) shows

strong easterlies in the upper to midtroposphere and weaker easterlies also in the lower troposphere in the west. Westerlies prevail in the mid- to lower troposphere in the central and eastern portions of the transect. In April (Figs. 3b and 3f), the centers of upward motion in the east and of subsidence in the west appear less intense than in January (Fig. 3a). The zonal component of the divergent part of the wind is also weaker, and again in the western part of the cross section not directed along the equator (Fig. 2b). The total zonal flow (Fig. 3f) is again strong easterly throughout the upper to midtroposphere, and in the western and eastern extremities of the cross section also in the lower layers. Strongest westerlies are found between about 60° and 100°E and somewhat above the surface; this contrasts with January (Fig. 3e) when the fastest westerlies are situated at 700 mb. In July (Figs. 3c and 3g), the ascending motion over Indonesia is weaker than in the other midseason months, and strongest lower-tropospheric convergence, upward motion, and upper-tropospheric divergence, are found near 60°E. Subsidence over the East African coast feeds mainly into an eastward divergent outflow centered on 700 mb; this passes into convergence to fuel the vigorous upward motion around 60°E, mainly upward of 700 mb. Thus a distinct zonal circulation cell is contained in the upper to midtroposphere between about 35° and 70°E. The cross section of total zonal flow (Fig. 3g) shows a strong westerly speed maximum centered around 700 mb and 60°–90°E, with easterlies aloft. In October (Figs. 3d and 3h), strong lower-tropospheric convergence, ascending motion, and upper-tropospheric divergence, are found over Indonesia, with divergent outflow toward the west and south (Fig. 2d). Subsidence prevails over the coast of East Africa, with upper-tropospheric convergent inflow from Central Africa and particularly from the east. Indeed in this season divergent easterly flow along the equator is well developed (Fig. 2d). Similar to July (Fig. 3c) the subsidence over the East African coast feeds primarily into divergent outflow eastward centered around 700 mb, where a core of strong westerlies extends from about 50° to 90°E. At about 60°–90°E the westerlies extend all the way to the surface.

The annual cycle of selected circulation indices (Fig. 4) complements the detailed documentation by the maps (Fig. 2) and the transects (Fig. 3) for the midseason months. For the Indonesian convection center, Fig. 4b illustrates the strongest ascending motion in boreal winter, when rainfall is also most abundant, and smallest negative values in boreal summer. For the western Indian Ocean domain (Fig. 4a) the annual cycle is less regular, but features strongest upward motion in the boreal summer half-year and subsidence in the latter part of the boreal winter half-year. Figures 4c and 4d depict for the upper troposphere the fastest easterlies in boreal summer and further illustrate that the divergent part is an order of magnitude smaller than the total zonal flow. In the mid- to lower troposphere (Figs. 4e–h) the annual cycle is broadly inverse to the upper troposphere (Figs. 2c and 2d), in that westerlies are fastest during the boreal summer half-year. Again, the divergent part (Figs. 4e and 4g) accounts for only a fraction of the total zonal flow (Figs. 4f and 4h). While there is overall vertical consistency from the 700- to the 850-mb level, the annual cycle of the total zonal flow at 850 mb (Fig. 2h) is complicated by double maxima of speed around May and October–November. This in turn is consistent with the evidence from surface ship observations (Hastenrath and Lamb 1979a, charts 14–25; Hastenrath et al. 1993), which bear out equatorial westerlies confined to April–May and October–November (Fig. 4i). These westerlies drive the likewise short-lived and intense eastward equatorial jet in the upper hydrosphere of the Indian Ocean (Wyrtki 1973; Hastenrath and Greischar 1989, 1991; Hastenrath et al. 1993) during the monsoon transitions in boreal spring and autumn.

In synthesis it becomes apparent from Figs. 2, 3, and 4 that there is only limited evidence for closed zonal circulation cells along the Indian Ocean equator. The Indonesian convection center is recognized as a major center of action, but the upper-tropospheric outflow is prevailingly meridional, changing direction between the boreal winter and summer seasons. Distinct easterly upper-tropospheric divergent flow along much of the Indian Ocean equator is found only in boreal autumn. Likewise, surface westerlies along the equator are limited to April–May and October–November. Furthermore, in boreal summer and autumn, the subsidence over the western Indian Ocean feeds into midtropospheric eastward outflow; a westerly speed maximum around 700 mb is coherent with surface westerlies at 60°–90°E in October. In fact, Figs. 2 and 3 offer indications of a zonal circulation cell along the equator at these longitudes only in boreal autumn, with upper-tropospheric divergent easterlies and surface westerlies tying into regions of ascending (decending) motion at the eastern (western) extremities of the Indian Ocean basin. A closed circulation cell is found in boreal summer confined to the western part of the cross section and contained in the upper to midtroposphere, further at variance with conventional notions.

4. Interannual variability

Circulation and climate are known to vary on interannual and longer timescales. The issue of decadal trends in the circulation over the equatorial Indian Ocean was explored using time series plots (not shown) of the indices defined in Fig. 1 for the 1958–97 period. No significant trends were found, so this section concentrates on interannual variability. This is studied from the 1958–97 correlations between representative indices in Tables 1–4, and from the stratification by three selection criteria (viz., high vs low SO phases, dry vs wet years at the coast of East Africa, and fast minus slow equatorial westerlies). These stratification analyses are presented in Figs. 5 and

6 by maps and cross sections in format analogous to the long-term mean (Figs. 2 and 3).

The correlations in Tables 1–4 provide a general orientation. Table 1 for January shows little correlation between the vertical motion at the western and eastern extremities of the Indian Ocean basin, W5ω and E5ω, although they are significantly correlated with the zonal flow in the upper and lower troposphere. Upper- and lower-tropospheric flow are strongly correlated and correlations are overall stronger with E5ω than with W5ω. The surface westerlies UEQ are significantly correlated with the lower to midtropospheric flow and vertical motion over Indonesia. The SOI is significantly correlated with the flow at various levels but not with vertical motion at the western and eastern extremities of the basin. The low correlation between W5ω and E5ω should recall Figs. 2a and 3a, which showed no upper-tropospheric flow connection from Indonesia to eastern Africa.

Table 2 for April again shows no correlation between

TABLE 1. Matrix of correlation coefficients for Jan 1958–97 (in hundredths). Refer to Fig. 1 for circulation indices. One and two asterisks indicate significance at the 5% and 1% levels, respectively. SOI is the pressure difference of Tahiti minus Darwin.

	W5ω	E5ω	2*du*	2*U*	7*du*	7*U*	8*du*	8*U*	7*ux*	8*ux*	UEQ	SOI
W5ω	—											
E5ω	+18	—										
2*du*	−42**	+39*	—									
2*U*	+32*	+36*	+01	—								
7*du*	−01	−59**	−35	−55**	—							
7*U*	−08	−50**	−32	−50**	+81**	—						
8*du*	+40**	−36*	−71**	−32*	−60**	+55*	—					
8*U*	+10	−44**	−48**	−32*	+52**	+74**	+72**	—				
7*ux*	+06	+16	+18	+10	+10	+02	−09	−21	—			
8*ux*	−18	+12	+27	−04	0	−22	−10	−32*	+09	—		
UEQ	−20	−55**	−35*	−30	+55**	+76**	+49**	+82**	−12	32*	—	
SOI	−05	−19	−15	−48**	+47**	+65**	+40*	+47**	+17	−12	+50**	—

TABLE 2. Matrix of correlation coefficients for Apr 1958–97 (in hundredths). Refer to Fig. 1 for circulation indices. One and two asterisks indicate significance at the 5% and 1% levels, respectively. SOI is the pressure difference of Tahiti minus Darwin. In addition, RAM is index of Apr–May rainfall at coast of equatorial East Africa.

	W5ω	E5ω	2*du*	2*U*	7*du*	7*U*	8*du*	8*U*	7*ux*	8*ux*	UEQ	SOI	RAM
W5ω	—												
E5ω	0	—											
2*du*	−48**	+53**	—										
2*U*	−04	+46**	+69**	—									
7*du*	−12	−64**	−43**	−60**	—								
7*U*	0	−36*	−37*	−47**	+66*	—							
8*du*	+45*	−70**	−73**	−50**	+56**	+35*	—						
8*U*	+33*	−47**	−59**	−56**	+53**	+78**	+71**	—					
7*ux*	+29	−34	−12	+12	+12	+04	+38	+14	—				
8*ux*	+28	−47*	−38	+18	+20	−12	+49*	+01	+36	—			
UEQ	+26	−43**	−62**	−60**	−64**	+70**	+66**	+80**	−01	+15	—		
SOI	−15	+12	+11	−22	+17	+38*	+03	+33*	−07	−37*	+24	—	
RAM	−14	−28	−09	+03	−05	−26	+16	−18	+10	+15	−01	−17	—

TABLE 3. Matrix of correlation coefficients for Jul 1958–97 (in hundredths). Refer to Fig. 1 for circulation indices. One and two asterisks indicate significance at the 5% and 1% levels, respectively. SOI is the pressure difference of Tahiti minus Darwin.

	W5ω	E5ω	2*du*	2*U*	7*du*	7*U*	8*du*	8*U*	7*ux*	8*ux*	UEQ	SOI
W5ω	—											
E5ω	+16	—										
2*du*	−20	+28	—									
2*U*	−18	+15	+18	—								
7*du*	+05	−33**	−43**	+08	—							
7*U*	+18	−07	−13	+15	+47**	—						
8*du*	+35*	−26	−81**	+15	+36*	+27	—					
8*U*	+22	−26	−53**	+07	+28	+65**	+73**	—				
7*ux*	+15	−15	−07	+20	+32	+50**	+06	+25	—			
8*ux*	+16	−09	−33*	+12	+35*	+24	+31*	+31	+33*	—		
UEQ	+16	−45**	−30	+09	+15	+48**	+45	+65**	+42**	+38*	—	
SOI	−07	−53**	−06	−19	+20	+06	−07	+10	+05	+15	+17	—

TABLE 4. Matrix of correlation coefficients for Oct 1958–97 (in hundredths). Refer to Fig. 1 for circulation indices. One and two asterisks indicate significance at the 5% and 1% levels, respectively. SOI is the pressure difference of Tahiti minus Darwin. In addition, RON is index of Oct–Nov rainfall at coast of equatorial East Africa.

	W5ω	E5ω	2*du*	2*U*	7*du*	7*U*	8*du*	8*U*	7*ux*	8*ux*	UEQ	SOI	RON
W5ω	—												
E5ω	−44**	—											
2*du*	−71**	+68**	—										
2*U*	−52**	+48**	+62**	—									
7*du*	+65**	−63**	−83**	−72**	—								
7*U*	+68**	−62**	−80**	−69**	+89**	—							
8*du*	+70**	−67**	−92**	−55**	+88**	+75**	—						
8*U*	+72**	−74**	−85**	−61**	+87**	+92**	+88**	—					
7*ux*	+40*	−44**	−66**	−43**	+61**	+57**	+69**	+63**	—				
8*ux*	+69**	−67**	−88**	−37*	+72**	+72**	+88**	+84**	+66**	—			
UEQ	+57**	−76**	−82**	−55**	+78**	+83**	+80**	+92**	+60**	+84**	—		
SOI	+47**	−43**	−66**	−50**	+64**	+56**	+69**	+63**	+46**	+62**	+58**	—	
RON	−56**	+41**	+66**	+36*	−61**	−64**	−65**	−72**	−38*	−68**	−80**	−55**	—

W5ω and E5ω, although both possess significant correlations with zonal flow at various levels. Noteworthy is the significant positive correlation between 8*ux* and 8*du*, indicating in the lower troposphere the tendency for a more eastward located speed maximum with faster westerly divergent flow. This characteristic grows more pronounced in later seasons. There is little correlation with the SO or rainfall at the coast of East Africa, in accordance with earlier findings (Hastenrath et al. 1993). Again, reference is invited to Figs. 2b and 3b to appreciate that the upper-tropospheric divergent outflow from Indonesia does not lead to equatorial East Africa.

Table 3 for July again lacks significant correlation between W5ω and E5ω, but correlations with the zonal flow at various levels are also weak. Even more pronounced than in April (Table 2) is the tendency for the westerly speed maximum in the lower troposphere (7*ux* and 8*ux*) to be located farther east with faster divergent and total westerly flow. E5ω but not W5ω possesses significant correlations with UEQ and SOI. Pertinent again is Fig. 2c, which portrays the prevailingly meridional divergent flow in the upper troposphere associated with the Indian summer monsoon.

In stark contrast to Tables 1–3, Table 4 for October contains highly significant correlations throughout. This should be appreciated with reference to Figs. 2d, 2h, and 3d, which bear out a distinct zonal circulation cell along the Indian Ocean equator, for this season of the year. Yet stronger than in the preceding seasons (Tables 2 and 3) are the correlations between the longitude of speed maximum (7*ux* and 8*ux*) and the divergent and total westerly wind in the lower troposphere. In addition to the very strong consistency between the various circulation indices, note the high correlations with UEQ, SOI, and RON. The extremely tight concurrent correlation between the surface westerlies over the equatorial Indian Ocean and the boreal autumn rains at the coast of East Africa has been pointed out before (Hastenrath et al. 1993).

From this exploration in Tables 1–4, it is found that overall strong correlations between the circulation indices materialize only in boreal autumn. More importantly, this is the only season in which the circulation over the Indian Ocean equator is strongly coupled with the phases of the SO, regional rainfall anomalies, and equatorial surface westerlies. Accordingly, the detailed stratification analyses shall be documented only for October by the maps and cross sections shown in Figs. 5 and 6. As indicated by the significant correlations of SOI with RON and UEQ and the even stronger correlation between RON and UEQ (Table 4), the stratifications according to these indices plausibly show major characteristics, and this is apparent in Figs. 5 and 6. The maps (Fig. 5) should be compared to the long-term mean maps (Figs. 2d and 2h), while the cross sections (Fig. 6) should be seen in context with the mean conditions (Figs. 3d and 3h).

Contrasting the high and low SO phases for the upper

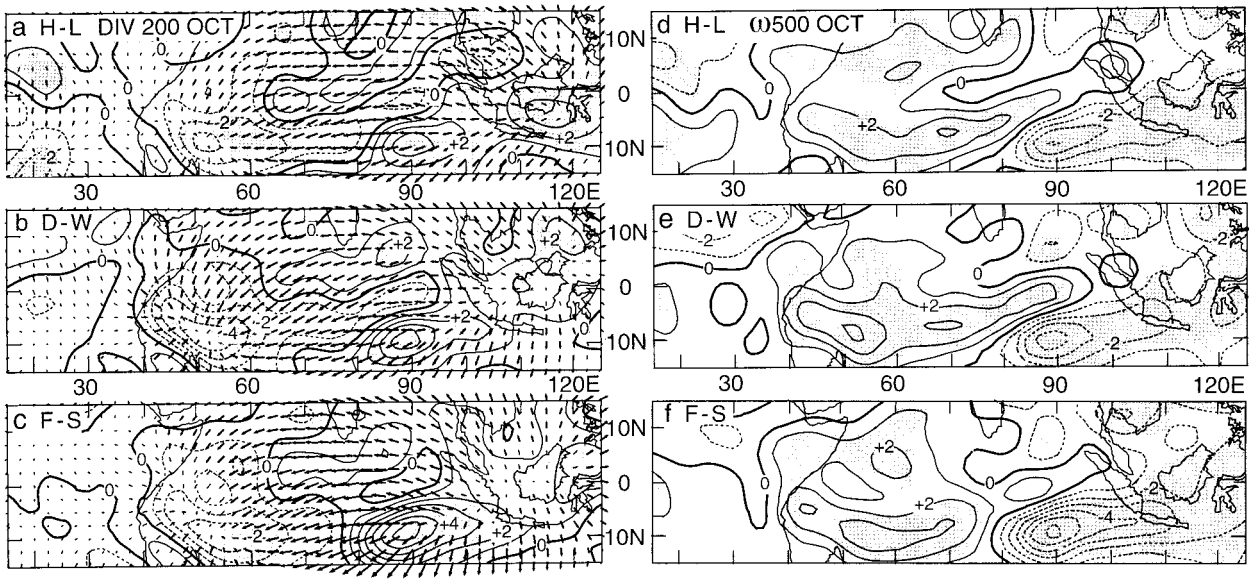

FIG. 5. Maps of Oct upper-air circulation differences between ensembles of extreme years: (a) and (d) high minus low SO phase (pressure index SOI); (b) and (e) dry minus wet conditions at the coast of East Africa (rain index RON); (c) and (f) years with fast minus years with slow surface westerlies over equatorial Indian Ocean [wind index UEQ (Oct)]. Maps (a)–(c) present the 200-mb field of difference in divergent wind with arrows scaled at 1° lat for 1 m s^{-1}. Divergence difference is shown with isoline spacing of 10^{-6} s^{-1} and dashed line indicates negative values. Maps (d)–(f) depict difference in vertical motion at 500 mb, with isoline spacing of 10^{-4} mb s^{-1}. Stippling and bold arrows indicate significance at the 5% level.

troposphere, Fig. 5a shows significantly enhanced divergence in the east, accelerated easterly flow along the equator, and stronger convergent inflow over eastern Africa. Concordant with this upper-tropospheric departure flow pattern, Fig. 5d bears out significantly intensified ascending motion in the east and decreased upward motion or enhanced subsidence over the southern and western Indian Ocean and eastern Africa. The stratification with regard to rainfall at the coast of East Africa (Figs. 5b and 5e) and the westerlies along the Indian Ocean equator (Figs. 5c and 5f) yields similar patterns.

The transects (Fig. 6) portraying the circulation in the zonal-vertical plane along the Indian Ocean equator should be appreciated in context with the maps in Fig. 5. In format analogous to Fig. 3, the transects Figs. 6a–c, contain the evidence on vertical motion, divergence, and zonal component of the divergent part of the wind field, while Figs. 6d–f pertain to the total zonal wind component. Figure 6a shows for the high versus the low SO phase in the eastern extremity of the transect, or Indonesia, significantly enhanced lower-tropospheric convergence, ascending motion, and upper-tropospheric divergence, as well as divergent outflow westward. At the western extremity of the Indian Ocean basin one finds significantly enhanced upper-tropospheric convergent inflow, subsidence, and divergence in the mid- to lower troposphere, as well as divergent outflow eastward. The cross section of the differences in the total zonal flow Fig. 6d shows significantly enhanced easterlies in the upper troposphere and accelerated westerlies in the lower layers. Again, the stratification with respect to East African rainfall (Figs. 5b and 5e) and equatorial westerlies (Figs. 5c and 5f) yields similar patterns.

In synthesis from Figs. 5 and 6 along with Tables 1–4, two contrasting regimes emerge. One of these regimes is characterized by an enhanced zonal circulation cell along the Indian Ocean equator, with accelerated equatorial surface westerlies, stronger upward motion over Indonesia and subsidence and deficient rainfall at the coast of East Africa. This regime is common in the high SO phase. The opposite regime features a weak zonal circulation cell including the equatorial westerlies, reduced ascending motion over Indonesia, and lesser subsidence and abundant rainfall at the East African coast, and this regime is common to the low SO phase. The zonal circulation cell and the strong relationships in its interannual variability are confined to the boreal autumn.

5. Conclusions

Bjerknes's (1969) seminal paper proposing a Walker circulation over the equatorial Pacific spawned a host of papers hypothesizing similar zonal–vertical circulation cells in the equatorial plane at other longitudes including the Indian Ocean. It seems tempting to consider that such equatorial circulation cells may play a role in regional climate anomalies. Prior to the NCEP–NCAR 40-Year Reanalysis, the dearth of upper-air information precluded the validation of such hypotheses. The motivation for the present study was twofold: to document the previously misunderstood upper-air cir-

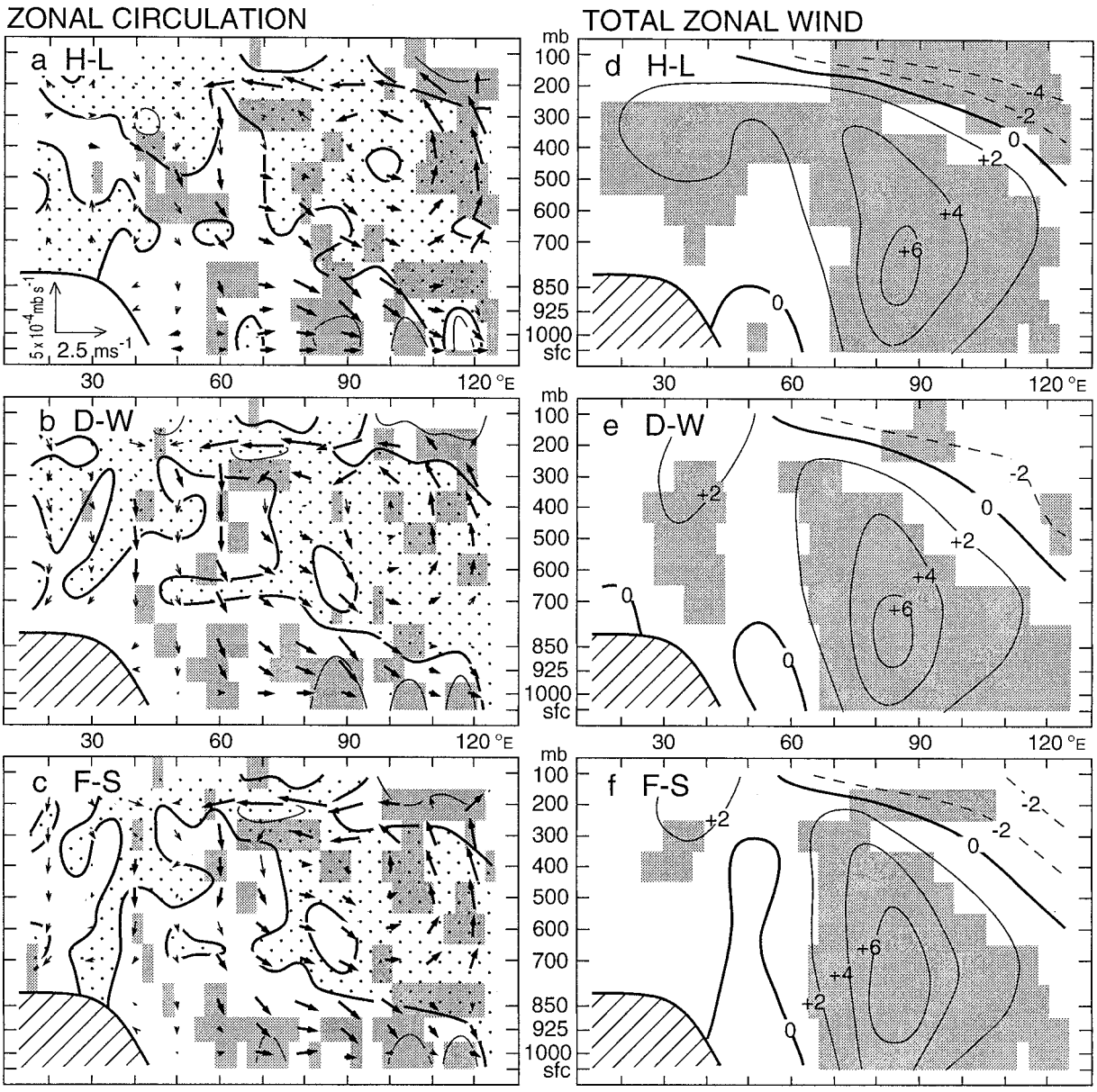

FIG. 6. Zonal–vertical cross sections of Oct circulation differences between ensembles of extreme years: (a) and (d) high phase minus low SO (pressure index SOI); (b) and (e) dry minus wet conditions at the coast of East Africa (rain index RON); (c) and (f) years with fast minus years with slow surface westerlies over equatorial Indian Ocean [wind index UEQ (Oct)]. Cross sections (a)–(c) present the difference in the zonal circulation, with inset in (a) indicating the scaling of arrows (m s^{-1}) for the divergent zonal wind component and (10^{-4} mb s^{-1}) for the omega vertical velocity. Stippling distinguishes domains of negative difference in divergence, with thin solid lines enclosing values beyond 1×10^{-6} s^{-1} in absolute amount (+ or −). Isotachs of total zonal wind component of 4 m s^{-1} are shown by dashed lines for the ensembles of the high (H) and low (L) phases of the SO in (a), for the dry (D) and wet (W) years in (b), and for the years with fast (F) and slow (S) equatorial westerlies in (c). Statistical significance at 5% level is indicated by dense dot raster for divergence and bold print for motion arrows. Cross sections (d)–(f) depict differences in total zonal wind component with isotach spacing of 2 m s^{-1} and dashed lines indicating negative values. Statistical significance at the 5% level is shown by stippling.

culation over the equatorial Indian Ocean better, and to explore the value of the new NCEP–NCAR upper-air analysis in relation to the surface climatic information. In context, the model assimilation basic to this dataset appears realistic. In the 1958–97 mean, ascending motion and upper-tropospheric divergence persist over Indonesia year round. In boreal winter, upper-tropospheric divergent outflow is directed from the southern Indian Ocean northwestward across the equator into southern Asia, and in summer from southern Asia southwestward into the Southern Hemisphere. During spring, divergent westerlies extend from Indonesia to the central Indian

Ocean. In boreal summer and autumn, a band of upper-tropospheric convergent inflow and midtropospheric subsidence develops over eastern Africa and the western Indian Ocean. In boreal autumn only, divergent/convergent easterlies blow from Indonesia along the equator into the upper-tropospheric convergence band over East Africa, and only then a closed zonal–vertical circulation cell materializes along the Indian Ocean equator, between the centers of ascending motion over Indonesia and of subsidence over equatorial East Africa and featuring westerlies in the lower layers.

No long-term trends could be detected, but the boreal autumn zonal circulation cell experiences marked interannual variability. A regime of intense zonal–vertical circulation along the equator features accelerated equatorial surface westerlies and enhanced subsidence and deficient rainfall at the coast of East Africa. In the high phase of the Southern Oscillation this regime is preferred. The regime of weak zonal circulation entails slow equatorial westerlies, decreased subsidence, and abundant rainfall in East Africa. The Southern Oscillation is significantly correlated with the equatorial westerlies and the boreal autumn rains at the East African coast, but the latter are even more tightly associated with the surface westerlies along the Indian Ocean equator.

Acknowledgments. This study was supported by NSF Grant ATM-9732673. At the University of Wisconsin, Dierk Polzin and Larry Greischar assisted me with the computations and graphics. I thank the anonymous reviewers for comments on an earlier version of this paper.

REFERENCES

Beltrando, G., and P. Camberlin, 1993: Interannual variability of rainfall in the eastern Horn of Africa and indicators of atmospheric circulation. *Int. J. Climatol.,* **13,** 533–546.

Bjerknes, J., 1969: Atmospheric teleconnections from the equatorial Pacific. *Mon. Wea. Rev.,* **97,** 163–172.

Chervin, R. M., and L. M. Druyan, 1984: The influence of ocean surface temperature gradient and continentality on the Walker Circulation. Part I: Prescribed tropical changes. *Mon. Wea. Rev.,* **112,** 1510–1523.

Farmer, G., 1988: Seasonal forecasting of the Kenya coast short rains, 1901–1984. *J. Climatol.,* **8,** 489–497.

Flohn, H., 1971: Tropical circulation patterns. *Bonner Meteor. Abh.,* **15,** 1–55.

Hastenrath, S., 1995: *Climate Dynamics of the Tropics.* 2d ed. Kluwer, 488 pp.

——, and P. J. Lamb, 1979a: *Surface Climate and Atmospheric Circulation.* Vol. 1, *Climatic Atlas of the Indian Ocean,* University of Wisconsin Press, 116 pp.

——, and ——, 1979b: *The Oceanic Heat Budget.* Vol. 2, *Climatic Atlas of the Indian Ocean,* University of Wisconsin Press, 110 pp.

——, and L. Greischar, 1989: *Uppper-Ocean Structure.* Vol. 3, *Climatic Atlas of the Indian Ocean,* University of Wisconsin Press, 273 pp.

——, and ——, 1991: The monsoonal current regimes of the tropical Indian Ocean: Observed surface flow fields and their geostrophic and wind-driven components. *J. Geophys. Res.,* **96** (C7), 12 619–12 633.

——, A. Nicklis, and L. Greischar, 1993: Atmospheric–hydrospheric mechanisms of climate anomalies in the western equatorial Indian Ocean. *J. Geophys. Res.,* **98** (C11), 20 219–20 235.

Hutchinson, P., 1992: The Southern Oscillation and the prediction of ''Der'' season rainfall in Somalia. *J. Climate,* **5,** 525–531.

Janowiak, J. E., 1988: An investigation of interannual rainfall variability in Africa. *J. Climate,* **1,** 240–255.

Kalnay, E., and Coauthors, 1996: The NCEP/NCAR 40-Year Reanalysis Project. *Bull. Amer. Meteor. Soc.,* **77,** 437–471.

Kousky, V. F., and C. F. Ropelewski, 1997: *The Tropospheric Seasonally Varying Mean Climate over the Western Hemisphere (1979–1995).* Atlas No. 3, NCEP/Climate Prediction Center, 135 pp.

Krishnamurti, T. N., 1971: Tropical east–west circulation during the northern summer. *J. Atmos. Sci.,* **28,** 1342–1347.

——, M. Kanamitsu, W. J. Koss, and J. D. Lee, 1973: Tropical east–west circulation during the northern winter. *J. Atmos. Sci.,* **30,** 780–787.

Mancuso, R. L., 1967: A numerical procedure for computing fields of streamfunction and velocity potential. *J. Appl. Meteor.,* **6,** 994–1001.

Newell, R. E., 1979: Climate and the ocean. *Amer. Sci.,* **67,** 405–416.

——, J. W. Kidson, D. G. Vincent, and G. J. Boer, 1972: *The General Circulation of the Tropical Atmosphere and Interactions with Extratropical Latitudes.* Vol. 1. The MIT Press, 258 pp.

——, ——, ——, and ——, 1974: *The General Circulation of the Tropical Atmosphere and Interactions with Extratropical Latitudes.* Vol. 2. The MIT Press, 371 pp.

Ogallo, L. J., 1988: Relationship between seasonal rainfall in East Africa and the Southern Oscillation. *J. Climatol.,* **8,** 31–43.

——, J. E. Janowiak, and M. S. Halpert, 1988: Teleconnection between seasonal rainfall over East Africa and global surface temperature anomalies. *J. Meteor. Soc. Japan, Ser. 2,* **66,** 807–821.

Quenouille, M. A., 1952: *Associated Measurements.* Butterworths, 242 pp.

Reverdin, G., D. Cadet, and D. Gutzler, 1986: Interannual displacement of convection and surface circulation over the equatorial Indian Ocean. *Quart. J. Roy. Meteor. Soc.,* **112,** 43–67.

Ropelewski, C. F., and M. S. Halpert, 1987: Global and regional precipitation patterns associated with the El Niño/Southern Oscillation. *Mon. Wea. Rev.,* **115,** 1606–1626.

——, and ——, 1989: Precipitation patterns associated with the high index phase of the Southern Oscillation. *J. Climate,* **2,** 268–284.

Woodruff, S., R. Slutz, R. Jenne, and P. Steurer, 1987: A Comprehensive Ocean–Atmosphere Data Set. *Bull. Amer. Meteor. Soc.,* **68,** 1239–1250.

——, S. Lubker, K. Wolter, S. Worley, and J. Elms, 1993: Comprehensive Ocean–Atmosphere Data Set (COADS) Release 1a: 1980–92. *Earth Syst. Monitor,* **4,** 1–8.

Wyrtki, K., 1973: An equatorial jet in the Indian Ocean. *Science,* **181,** 262–264.